

# Signatures of Quantum Chaos in Wave Functions Structure for Multi-well 2D Potentials

V. P. Berezovoj<sup>+</sup>, Yu. L. Bolotin<sup>+</sup>, V. A. Cherkaskiy<sup>+1)</sup>

<sup>+</sup> A.I.Akhiezer Institute for Theoretical Physics, National Science Center "Kharkov Institute of Physics and Technology", Akademicheskaya Str. 1, 61108 Kharkov, Ukraine

Submitted 1 November 2003

We propose a new approach to investigation of quantum manifestations of classical stochasticity (QMCS) in wave functions structure, which can be realized in potentials with two and more local minima. The main advantage of the proposed approach is the possibility to detect QMCS in comparison not different wave functions, but different parts of the same wave function. Efficiency of the approach is demonstrated for two potentials: surface quadrupole oscillations (QO) and lower umbilic catastrophe (UC)  $D_5$ .

PACS: 05.45.Mt, 05.45.Pq

Energy spectra and eigenfunctions of classically non-integrable systems represent the main object of search for QMCS [1, 2, 3]. It should be pointed out that in analysis of QMCS in the energy spectra the principal role was given to statistical characteristics, i.e. quantum chaos was treated as property of a group of states. In contrast, the choice of a stationary wave function as a basic object of investigation, relates quantum chaos to an individual state. Usual procedure of search for QMCS in wave function implies investigation of distinction in its structure below and above the classical energy of transition to chaos (or other parameters of regularity-chaos transition). Such procedure meets difficulties connected with necessity to separate QMCS from modifications of wave functions structure due to trivial changes in its quantum numbers. Up to present time correlations between peculiarities of the classical motion and structure of wave functions were studied mostly for billiard-type systems [4, 5, 6]. For Hamiltonian systems with non-zero potential energy QMCS were studied either for model wave functions [7] or for potential energy surfaces (PES) with simple geometry [8]. Till now there is practically no information on wave functions structure for generic Hamiltonian systems, including multi-well potentials. Such systems allow existence of the mixed state (MS): different (regular or chaotic) classical regimes coexist in different local minima at fixed energy [9, 10]. Aim of our work is to show, that such systems represent optimal object for investigation of QMCS in wave functions structure. Wave functions of MS allow to find QMCS in comparison not different eigenfunctions, but different parts of the same wave function, situated in different regions of configuration space (corresponding

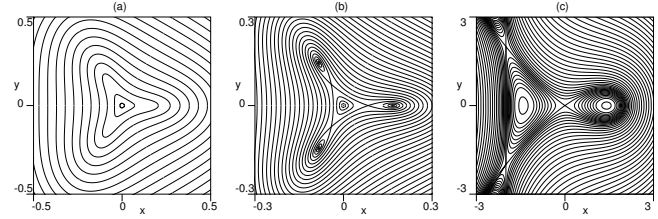


Figure 1: The level lines of the QO potential (6b) for  $W = 13$  (a),  $W = 18$  (b), and for the UC  $D_5$  (7) with  $a = 2$  (c).

to different local minima of the potential).

Let us demonstrate this possibility for MS, generated by the deformation potential of surface QO of atomic nuclei [11] and lower UC  $D_5$  [12]. It can be shown [13], that using only the transformation properties of the interaction, the QO potential takes the form

$$U_{QO}(a_0, a_2) = \sum_{m,n} C_{mn} (a_0^2 + 2a_2^2)^m a_0^n (6a_2^2 - a_0^2)^n \quad (1)$$

where  $a_0$  and  $a_2$  are internal coordinates of nuclear surface undergoing the QO

$$R(\theta, \varphi) = R_0 \{ 1 + a_0 Y_{2,0}(\theta, \varphi) + a_2 [Y_{2,2}(\theta, \varphi) + Y_{2,-2}(\theta, \varphi)] \} \quad (2)$$

Since in the construction of (1) only transformation properties of interaction play role, this expression describes potential energy of surface QO of a charged liquid drop of any nature (for example, a metal cluster [14]), containing specific character of the interaction only in the coefficients  $C_{mn}$ . Restricting ourselves with the terms of fourth order in the deformation and assuming equality of masses for the two independent direc-

<sup>1)</sup>e-mail: cherkaskiy@ktp.kharkov.ua

tions, we get the following  $C_{3v}$ -symmetric Hamiltonian

$$H = \frac{p_x^2 + p_y^2}{2m} + U_{QO}(x, y; a, b, c) \quad (3)$$

where

$$U_{QO}(x, y; a, b, c) = \frac{a}{2}(x^2 + y^2) + b(xy^2 - \frac{1}{3}x^3) + c(x^2 + y^2)^2 \quad (4)$$

$$x = a_0, y = \sqrt{2}a_2, a = 2C_{10}, b = 3C_{01}, c = C_{20}$$

Let us introduce the dimensionless variables

$$(x, y) = l_0(\bar{x}, \bar{y}), (p_x, p_y) = p_0(\bar{p}_x, \bar{p}_y), E = \varepsilon_0 \bar{E} \quad (5a)$$

$$l_0 = \frac{b}{c}, p_0 = \sqrt{m \frac{b^4}{c^3}}, \varepsilon_0 = \frac{b^4}{c^3} \quad (5b)$$

In the variables  $(\bar{x}, \bar{y})$  (further we will drop the bar line) the Hamiltonian (3) has the form

$$H = \frac{p_x^2 + p_y^2}{2m} + U_{QO}(x, y; W) \quad (6a)$$

$$U_{QO}(x, y; W) = \frac{1}{2W}(x^2 + y^2) + xy^2 - \frac{1}{3}x^3 + (x^2 + y^2)^2 \quad (6b)$$

Hamiltonian (6a) and corresponding equations of motion depend only on  $W = b^2/(ac)$ , which is the unique dimensionless parameter, that can be constructed from  $a, b$  and  $c$ , and it completely determines the PES [Fig.1(a),(b)]. Region  $0 < W \leq 16$  includes potentials with only one critical point — minimum in the origin [Fig.1(a)], corresponding to spherically symmetric equilibrium shape of the nucleus (or liquid charged drop). For  $W > 16$  the PES has seven critical points: four minima (one central and three peripheral) and three saddles, separating the peripheral minima from the central one [Fig.1(b)]. In this Letter we consider in details the case  $W = 18$ , when the potential (6b) has four minima with the same value  $E_{min} = 0$  and the saddle energies  $E_S = 1/20736$ . It was shown [9], that the critical energy of transition to chaos  $E_{cr}$  has different values for different minima:  $E_{cr} = E_S/2$  for the central minimum and  $E_{cr} = E_S$  for the peripheral ones. It means, that for  $E_S/2 < E < E_S$  regular and chaotic trajectories coexist and are separated not in phase, but in configuration space, resulting in the phenomenon of MS.

MS is a common case for multi-well potentials. According to catastrophe theory, a wide class of multi-well 2D polynomial potentials can be generated by germs of lower UC of types  $D_5, D_6^\pm, D_7$  from the Thom catastrophes list, affected by certain perturbation [12]. To

demonstrate the proposed approach we consider, apart from the QO potential (6b), a lower UC  $D_5$ , described by germ  $x^4/4 + y^2x$  with perturbation  $bx^2 - ay^2$ . This potential has only two local minima and three saddles [Fig.1(c)], and therefore it is the simplest potential, where MS is observed. Under the Maxwell condition  $b = a^2/4$  the energies of all the saddles are the same, and energies of all the local minima too. We will consider the case  $a = 2, b = 1$

$$U_{D_5}(x, y) = \frac{x^4}{4} + xy^2 + 2y^2 - x^2 \quad (7)$$

when all  $E_{min} = -1$  and all  $E_S = 0$ , and MS is observed in the energy region  $-1/2 < E_{MS} < 0$ .

Calculation of quasiclassical part of the spectrum for systems with multi-well PES requires appropriate numerical methods. Matrix diagonalization (MD) method is attractive for the Hamiltonians with eigenfunctions, that do not differ too much from the basis functions. However this numerical procedure becomes less attractive (or even not efficient at all) at the transition to PES of complicated topology (multi-well potentials). In particular, the diagonalization of the QO Hamiltonian (6a) with  $W > 16$  in the harmonic oscillator basis requires so large number of the basis functions, that goes beyond the limits of the computation power. In this case the attractive alternative to the MD may become the spectral method (SM) in the form, proposed by Feit et al. [15].

Numerical solution of the stationary Schrödinger equation

$$\left[ -\frac{\hbar^2}{2}\Delta + U(x, y) \right] \psi_n(x, y) = E_n \psi_n(x, y) \quad (8)$$

by the SM requires computation of the correlation function

$$P(t) = \int dx dy \psi_0^*(x, y) \psi(x, y, t) \quad (9)$$

where  $\psi(x, y, t)$  represents a numerical solution of the corresponding time-dependent Schrödinger equation with an arbitrary initial condition  $\psi_0(x, y) = \psi(x, y, t = 0)$ . The solution  $\psi(x, y, t)$  can be accurately generated with the help of the split operator method

$$\psi(x, y, t + \Delta t) = e^{i \frac{\hbar^2 \Delta t \nabla^2}{4}} e^{-i \Delta t U(x, y)} e^{i \frac{\hbar^2 \Delta t \nabla^2}{4}} \psi(x, y, t) + O(\Delta t^3) \quad (10)$$

where  $\exp(i \hbar^2 \Delta t \nabla^2 / 4) \psi(x, y, t)$  is evaluated with the help of the band-limited Fourier series representation

$$\psi(x, y, t) = \sum_{m=-N/2+1}^{N/2} \sum_{n=-N/2+1}^{N/2} \psi_{mn}(t) e^{\frac{2\pi i}{L_0}(mx+ny)} \quad (11)$$

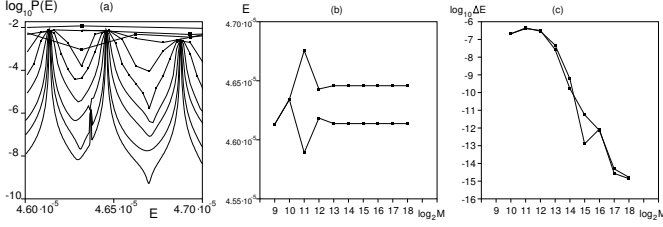


Figure 2: Determination of two close energy levels  $E_n$  and  $E_{n+1}$  in the QO potential (6b) with  $W = 18$  and different number of time steps  $M = 2^k, k = 9, 10, \dots, 18$ : (a) - absolute value of  $P^{(k)}(E)$  in log scale, (b) - values of  $E_n^{(k)}$  and  $E_{n+1}^{(k)}$ , (c) - consecutive corrections  $E_n^{(k-1)} - E_n^{(k)}$  and  $E_{n+1}^{(k-1)} - E_{n+1}^{(k)}$ .

where  $N$  is the number of grid points along a grid line and  $L_0$  is the grid length.

From the other hand, the solution  $\psi(x, y, t)$  can be expressed as a linear superposition of eigenfunctions  $\psi_n(x, y)$  of (8)

$$\psi(x, y, t) = \sum_n a_n \psi_n(x, y) \exp(-iE_n t/\hbar) \quad (12)$$

We assume no degenerate states in the decomposition (12), which can always be achieved by certain choice of the initial condition  $\psi_0(x, y)$ . Using (12) in (9), we obtain

$$P(t) = \sum_n |a_n|^2 \exp(-iE_n t/\hbar) \quad (13)$$

The Fourier transform of (13)

$$P(E) = \frac{1}{T} \int_0^T dt e^{i\frac{Et}{\hbar}} P(t) w(t) = \sum_n |a_n|^2 \delta_T(E - E_n) \quad (14)$$

where

$$\delta_T(E) = \frac{1}{T} \int_0^T dt w(t) e^{i\frac{Et}{\hbar}} = \frac{e^{i\frac{ET}{\hbar}} - 1}{i\frac{ET}{\hbar}} - \frac{1}{2} \left[ \frac{e^{i(\frac{ET}{\hbar} + 2\pi)} - 1}{i(\frac{ET}{\hbar} + 2\pi)} + \frac{e^{i(\frac{ET}{\hbar} - 2\pi)} - 1}{i(\frac{ET}{\hbar} - 2\pi)} \right] \quad (15)$$

and  $w(t) = 1 - \cos(2\pi t/T)$  is the Hanning window function. The plot for  $P(E)$  displays a set of sharp local maxima at  $E = E_n$  [Fig.2(a)], where  $E_n$  are the energy eigenvalues of (8). Once the eigenvalues are known, the corresponding eigenfunctions can be computed by numerically evaluating the integrals

$$\psi_n(x, y) = \frac{1}{T} \int_0^T dt \psi(x, y, t) w(t) e^{i\frac{E_n t}{\hbar}} \quad (16)$$

This procedure is very efficient, when implemented with the help of the fast Fourier transform algorithm (FFT),

and very accurate, since the spatial derivatives are approximated to  $N$ th order in  $\Delta x = \Delta y = L_0/N$ .  $L_0$  and  $N$  must be chosen large enough, and  $\psi_0(x, y)$  sufficiently fast decaying with its Fourier components, in order to assure that  $\psi(x, y, t)$  is negligible on the grid boundaries both in coordinate and reciprocal spaces. The sampling interval  $\Delta t$  limits the spectral bandwidth  $\Delta E_{max} = \pi\hbar/\Delta t$  of a function that can be represented by a Fourier series determined by sampled values. Therefore  $\Delta t$  should be chosen small enough to accommodate the necessary number of energy levels, or  $\Delta E_{max} > \Delta U_{max}$ , where  $\Delta U_{max}$  is the maximum excursion of the potential. Since the potential (6b) is unbounded, it is necessary to put an appropriate cutoff in order to apply the SM. If the wave function  $\psi(x, y, t)$  is generated over a total time  $T = M\Delta t$ , the minimum separation in energy levels that can be resolved is  $\Delta E_{min} = \pi\hbar/T$ , which also provides an estimate of the accuracy with which individual eigenvalues can be determined from the numerically computed  $P(E)$  (14) without the aid of lineshape fitting techniques. Such techniques, however, may improve the eigenvalues accuracy by roughly two orders of magnitude. Fig.2 shows the typical shape of  $P(E)$  [Fig.2(a)] and the corresponding two close energy levels [Fig.2(b)], calculated for increasing  $M = 2^k, k = 9, 10, \dots, 18$ , using the single-line fit. For  $k = 9, 10$  the levels look as one, at  $k \geq 11$  they are resolved, and for  $k > 13$  their values change much less than the level spacing. Fig.2(c) shows the differences between the eigenvalues, calculated with given  $M = 2^k$  and the more accurate, calculated with  $M = 2^{k+1}$  — the procedure converges fast indeed, displaying the saturation in accuracy.

In applying the SM, a preponderant fraction of the computer time goes to the generation of the  $\psi(x, y, t)$ , and most of that time in turn is invested in FFT computations, so the overall calculation time for our 2D problems scales as  $MN^2 \ln N$ . We performed our calculations with  $N = 512$  and  $M = 65536$ , which allowed to obtain for reasonable time about  $10^2$  eigenfunctions with sufficient accuracy and high coordinate resolution to allow their detailed analysis. The scaled Planck's constant  $\hbar$  is an arbitrary parameter and is chosen to obtain the desired number of energy levels.

Let us now discuss the results obtained for the potentials  $U_{QO}$  and  $U_{D5}$ . In the former case for  $W < 16$  the only possibility to detect the QMCS in the wave function structure is to look how it changes as energy grows. As was shown in [16], for  $4 < W < 16$  energy region of chaotic motion is bounded from both sides:  $E_{cr1} < E_c < E_{cr2}$ , which means the regularity-chaos-regularity (R-C-R) transition at energies  $E_{cr1}$  and  $E_{cr2}$

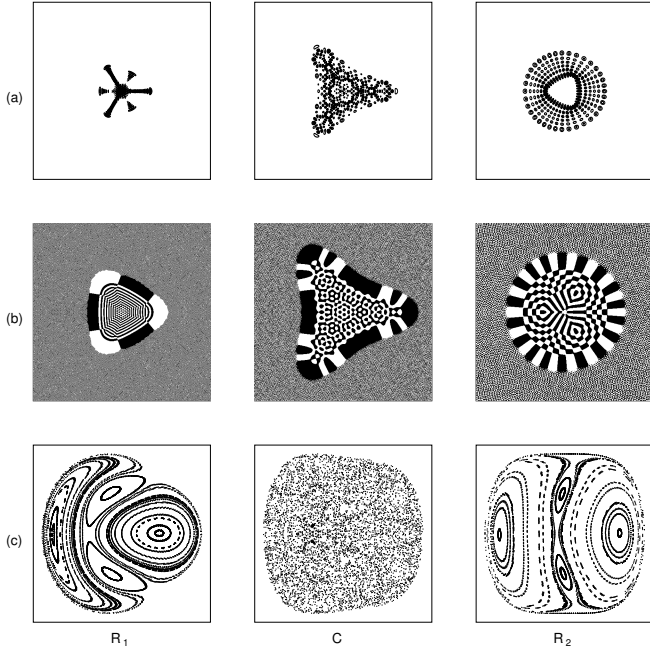


Figure 3: The R-C-R transition in the QO potential (6b) with  $W = 13$ .

respectively. We will distinguish three energy regions: low-energy regular  $R_1(E < E_{cr1})$ , chaotic  $C(E_{cr1} < E < E_{cr2})$  and high-energy regular  $R_2(E > E_{cr2})$ . For the considered case  $W = 13$  the R-C-R transition is observed at critical energies  $E_{cr1} = 8 \cdot 10^{-5}$  and  $E_{cr2} = 8.4 \cdot 10^{-2}$  respectively. Fig.3 shows the changes in the structure of level lines of  $|\psi_n|^2$  [Fig.3(a)] and the corresponding nodal domains picture [Fig.3(b)], clearly correlating with the character of the classical motion, displayed in the corresponding Poincaré surfaces of section [Fig.3(c)].

The considered possibility corresponds to the traditional approach in search of QMCS in the wave function structure. Existence of the MS, at  $W > 16$  for the QO potential [Fig.4(a)] or in the UC  $D_5$  potential [Fig.4(b)], opens a new possibility. Comparing the structure of the eigenfunction in central and peripheral minima of the QO potential [Fig.4(c)], or in left and right minima of the UC  $D_5$  potential [Fig.4(d)], it is evident that the nodal structures of the regular part and the chaotic part of the eigenfunction are clearly different:

- i) within the classically allowed region the nodal domains of the regular part of the wave function form a well recognizable checkerboard-like pattern [1]; nothing similar can be observed for the chaotic part;
- ii) the nodal lines of the regular part exhibit crossings or very tiny quasicrossings; in the chaotic part the nodal

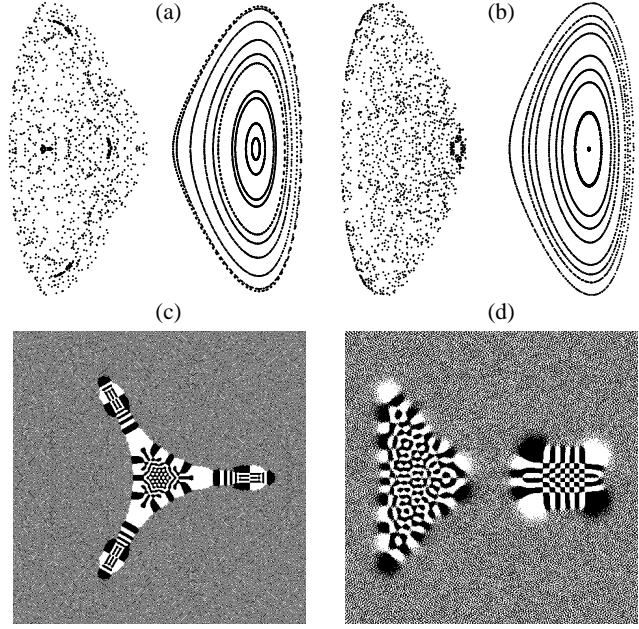


Figure 4: The MS in the QO potential (a),(c) and in the  $D_5$  UC (b),(d): (a),(b) – Poincaré surfaces of section, (c),(d) – nodal domains of the eigenfunctions.

lines quasicrossings have significantly larger avoidance ranges;

- iii) while crossing the classical turning line  $U(x, y) = E_n$ , the nodal lines structure of the regular part immediately switches to the straight nodal lines, going to infinity, which makes the turning point line itself easily locatable in the nodal domains structure; in the chaotic part an intermediate region exists around the turning line, where some of the nodal lines pinch-off, making transition to the classically forbidden region more gradual and not so manifesting in the nodal structure.

In conclusion we remark that the Hamiltonian system with multi-well PES represents a realistic model, describing the dynamics of transitions between different equilibrium states, including such important cases, as chemical reactions and nuclear fission. Existence of the MS must essentially determine dynamics of the physical processes in such systems, for instance the quantum assistance tunnelling. We demonstrated a possibility to observe the QMCS in an individual quantum mechanical state — an eigenfunction of the MS. Further analysis implies investigation of the eigenfunction amplitude distribution, nodal lines quasicrossings avoidance range distribution, and the wave packets dynamics. Another interesting perspective is to study relevance of the Berry-Robnik formula for the energy levels spacings

distribution in the MS and to investigate the nodal domains and the nodal lines statistics.

- 
1. M. C. Gutzwiller, *Chaos in Classical and Quantum Mechanics* (Springer Verlag, New-York, 1990).
  2. F. Haake, *Quantum Signatures of Chaos* (Springer Verlag, Berlin, 1992).
  3. H.-J. Stockmann, *Quantum Chaos. An Introduction.* (Cambridge University Press, 1999).
  4. M. V. Berry, J. Phys. **A10**, 2083 (1977).
  5. S. W. McDonald, A. N. Kaufman, Phys. Rev. **A37**(8), 3067 (1988).
  6. B. Li and M. Robnik, J. Phys. **A: Math. Gen.** **28**, 2799 (1995)& **29**, 4387 (1996).
  7. W. E. Bies, E. J. Heller, J. Phys. **A35**, 5673 (2002).
  8. R. M. Stratt, N. C. Handy, W. H. Miller, J. Chem. Phys. **71**(8), 3311 (1979).
  9. Yu. L. Bolotin, V. Yu. Gonchar, E. V. Inopin, Yad. Fiz. **45**, 350, (1987).
  10. V. P. Berezovoj, Yu. L. Bolotin, V. Yu. Gonchar, M. Ya. Granovsky, Particles & Nuclei **34**(2), 388 (2003).
  11. J. Eizenberg, W. Greiner, *Nuclear theory, V.1, Nuclear Models* (North-Holland, Amsterdam-London, 1970).
  12. R. Gilmore, *Catastrophe Theory* (John Wiley & Sons, New York, 1981).
  13. V. Mozel and W. Greiner, Z.Phys. **217**, 256 (1968).
  14. W. A. Saunders, Phys. Rev. Lett. **64**, 3046 (1990).
  15. M. D. Feit, J. A. Fleck, Jr., and A. Steiger, Journ. Comp. Phys. **47**, 412 (1982).
  16. Yu. L. Bolotin et al., Particles & Nuclei, **20**, 878 (1989).